DOI: 10.1002/ange.201409519

Theranostics

ZnO-Functionalized Upconverting Nanotheranostic Agent: Multi-Modality Imaging-Guided Chemotherapy with On-Demand Drug Release Triggered by pH**

Yinghui Wang, Shuyan Song, Jianhua Liu, Dapeng Liu, and Hongjie Zhang**

Abstract: *Limited therapeutic efficiency and severe side effects in patients are two major issues existing in current chemotherapy of cancers in clinic. To design a proper theranostic platform seems thus quite needed to target cancer cells accurately by bioimaging and simultaneously release drugs on demand without premature leakage. A novel ZnO-functionalized upconverting nanotheranostic platform has been fabricated for clear multi-modality bioimaging (upconversion luminescence (UCL), computed tomography (CT), and magnetic resonance imaging (MRI)) and specific pH-triggered on-demand drug release. In our theranostic platform multi-modality imaging provides much more detailed and exact information for cancer diagnosis than single-modality imaging. In addition, ZnO can play the role of a "gatekeeper" to efficiently block the drug in the mesopores of the as-prepared agents until it is dissolved in the acidic environment around tumors to realize sustained release of the drug. More importantly, the biodegradable ZnO, which is non-toxic against normal tissues, endows the as-prepared agents with high therapeutic effectiveness but very low side effects. These findings are of great interests and will inspire us much to develop novel effective imaging-guided on-demand chemotherapies in cancer treatment.*

Interest in constructing theranostic nanoplatforms with concurrent diagnostic and therapeutic capabilities has recently grown in the field of nanomedicine since it offers great opportunities in the fight against various major diseases, such as cancer. Imaging probes, as one of the most important parts of the theranostic nanoplatform, should simultaneously fulfill different levels of imaging, from the cell to the whole body, to offer detailed tumor characteristics for clinical diagnostics. However, single-modality imaging cannot meet the high diagnostic requirements as every imaging method (e.g., optical imaging, CT, and MRI) has its inherent defects rooted in limited sensitivity, resolution or imaging depths.[1] To resolve this problem, multiple imaging probes have been integrated into one single system for achieving multi-modality imaging despite some severe drawbacks including complicated synthetic procedures and heterogeneous nanostructures.[2] In response, lanthanide-doped upconverting nanoparticles (UCNPs), may be ideal alternatives for constructing multifunctional bioprobes through doping with different rare-earth ions without additional modification of other functionalities owing to their rich optical and magnetic properties as well as strong X-ray attenuation.[3–5]

Besides multi-modality imaging for diagnosis, therapeutic applications of UCNPs have also been studied intensively in the past years.[5h,6] For example, UCNPs with mesoporous silica shell (dubbed as UCNPs@mSiO_2) have been employed as anti-cancer drug nanocarriers in malignant tumor treatment.[7] However, it is hard to prevent premature release of anticancer drugs before they reach the tumor, resulting in the poor therapeutic efficacy and cytotoxicity. One promising strategy to tackle this issue is to explore a stimuli-responsive drug-delivery system, which can realize the on-demand drug release triggered by specific external stimuli, including pH,[8] light,[3a,9] and temperature.[10] Recently, a study on hollow/mesoporous silica coated UCNPs drug nanocarriers with high pH sensitivity has received more attention because of the notable difference between normal tissues (pH 7.4) and tumors (pH < 5.5).[11] Unfortunately, in the absence of a "gatekeeper" on their surfaces, there are still more than 20% of the drugs pre-released from the nanocarriers at pH 7.4. In consideration of the high desire of developing UCNPs@m-SiO_2 nanocarriers that possess highly effective pH sensitivity as well as a non-toxic "gatekeeper" to prevent the premature drug release, ZnO nanoparticles become the ideal candidate that are easy to be fabricated, inexpensive, and highly responsive to acids (stable at pH 7.4 but rapidly dissolved while pH < 5.5).[12] More importantly, biodegradable ZnO is non-toxic towards normal tissues but cytotoxic towards tumors after dissolution. However, to the best of our knowledge, construction of theranostic nanoplatforms combining multi-modality bioimaging and pH-triggered chemotherapy seems still unsuccessful in the literature to date.

Herein, we have developed a multifunctional nanotheranostic agent with UCNPs ($NaYF_4$: 20% Yb^{3+}, 2% Er^{3+}/$NaGdF_4$: 2% Yb^{3+}) as the core for the UCL/CT/MRI tri-modality imaging, and a mesoporous silica layer as the outer shell with ZnO as "gatekeeper" for pH-triggered drug delivery, designated as UCNPs@mSiO_2-ZnO (Scheme 1).

[*] Y. H. Wang, S. Y. Song, D. P. Liu, Prof. H. J. Zhang
State Key Laboratory of Rare Earth Resource Utilization
Changchun Institute of Applied Chemistry (CIAC)
Chinese Academy of Sciences (CAS)
Changchun, 130022 (P. R. China)
E-mail: liudp@ciac.ac.cn
hongjie@ciac.ac.cn
J. H. Liu
Department of Radiology
The Second Hospital of Jilin University
Changchun, 130041 (P. R. China)

[**] Financial support by NSFC (grant numbers 51372242, 51272249, 91122030, 21210001, and 21221061) and National Key Basic Research Program of China (grant number 2014CB643802).
Supporting information for this article is available on the WWW under http://dx.doi.org/10.1002/anie.201409519.

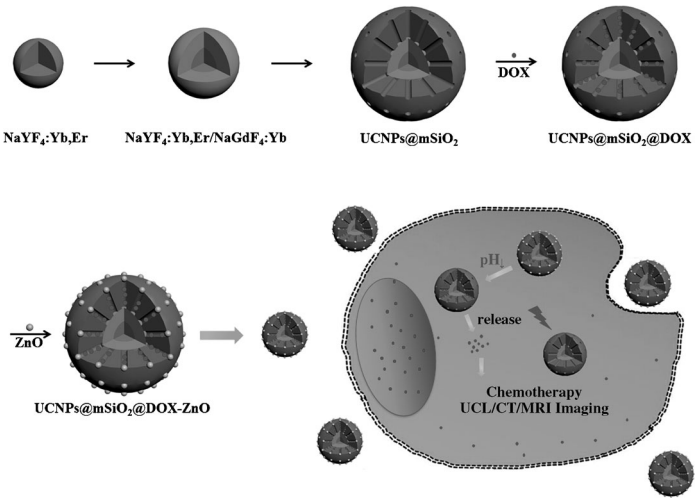

Scheme 1. Synthesis of UCNPs@mSiO$_2$@DOX-ZnO for multi-modality bioimaging guided pH-triggered chemotherapy.

The as-prepared UCNPs are in a hexagonal phase and possess uniform morphology (Figures S1 and S2 in the Supporting Information). The HAADF-STEM (high angle annular dark field scanning transmission electron microscopy) image and the line scanning profiles further confirm its core–shell structure (Figure S3a). The TEM image in Figure 1a shows that the silica coating process on UCNPs is successful and the as-obtained UCNPs@mSiO$_2$ is still uniform in size and monodisperse. The low-angle XRD analysis and nitrogen

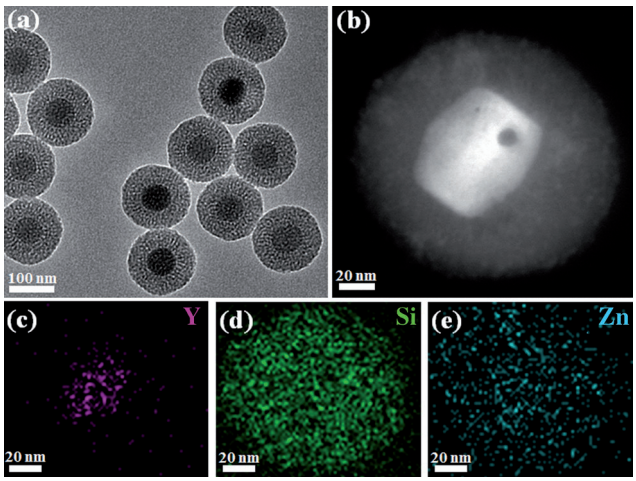

Figure 1. a) TEM image of UCNPs@mSiO$_2$, b) HADDF-STEM image of UCNP@mSiO$_2$-ZnO, and c–e) EDS mapping of Y, Si, and Zn according to the image in (b).

adsorption–desorption isotherm (Figures S5 and S6) clearly indicate its highly ordered mesoporous structure. The high-resolution TEM and FTIR characterization demonstrate that these mesopores can be successfully blocked by the pre-prepared NH$_2$-functionalized ZnO quantum dots[12a] as "gatekeeper" using a carbodiimide cross-linking reaction with the COOH-anchored UCNPs@mSiO$_2$ (Figures S3, S4, and S7). This result has been also proved by HAADF-STEM (Figure 1b) and elemental mapping analysis (Figure 1c to e).

No obvious change in the UCL wavelength and sharpness is observed before and after coating ZnO quanum dots on the surface of UCNPs@mSiO$_2$ (Figure S8). The characteristic UCL emission can be used as the output signals to realize UCL imaging. Then cellular uptakes of UCNPs@mSiO$_2$-ZnO were investigated by a modified inverted fluorescence microscope equipped with a 980 nm infrared laser. After incubation with UCNPs@mSiO$_2$-ZnO for 4 h, the HeLa cells showed evident UCL signals (Figure 2a). The UCNPs@mSiO$_2$-ZnO was mainly located in the cytoplasm and perinuclear regions, indicating the successful penetration of UCNPs@mSiO$_2$-ZnO into the cell membrane of living HeLa cells. The internalized process of UCNPs@mSiO$_2$-ZnO by the cells was verified through the UCL imaging

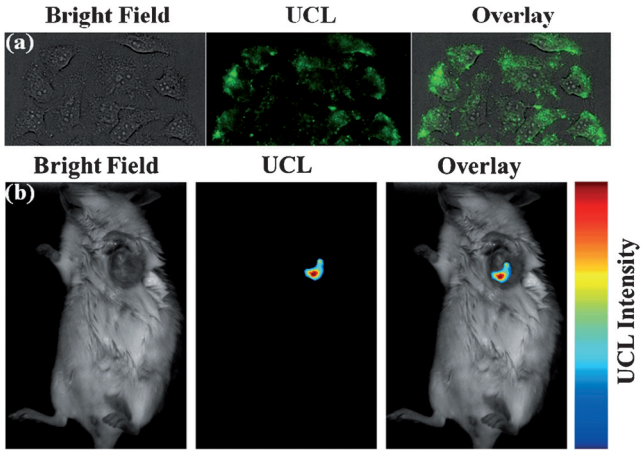

Figure 2. a) Inverted fluorescence microscope images of HeLa cells stained with UCNPs@mSiO$_2$-ZnO at 37 °C. b) In vivo UCL imaging of a tumor-bearing Balb/c mouse after injection of UCNPs@mSiO$_2$-ZnO at the tumor site. Overlay of a luminescence image and a bright field image were also shown.

(Figure S9). Then, we intratumorally injected UCNPs@mSiO$_2$-ZnO into the tumor site, and imaged them by a modified in vivo Maestro whole-body imaging system. A strong UCL signal began to arise from the location where UCNPs@mSiO$_2$-ZnO was injected (Figure 2b), but no autofluorescence was detected elsewhere. Such results demonstrate that UCNPs@mSiO$_2$-ZnO is able to be employed for UCL imaging in vitro and in vivo.

As known, in vivo UCL imaging provides only imprecise anatomical and physiological information restricted by the penetration depth of lights unless the simultaneous integration with CT. So we compared the CT contrast efficacy of UCNPs@mSiO$_2$-ZnO with that of iobitridol (a tradiational iodine-based CT contrast agent currently used in clinic). As shown in Figure 3a and b, UCNPs@mSiO$_2$-ZnO shows much brighter CT images than iobitridol at equivalent concentrations ascribed to its appropriate K-edge and high atomic number. Furthermore, after intratumoral injection of

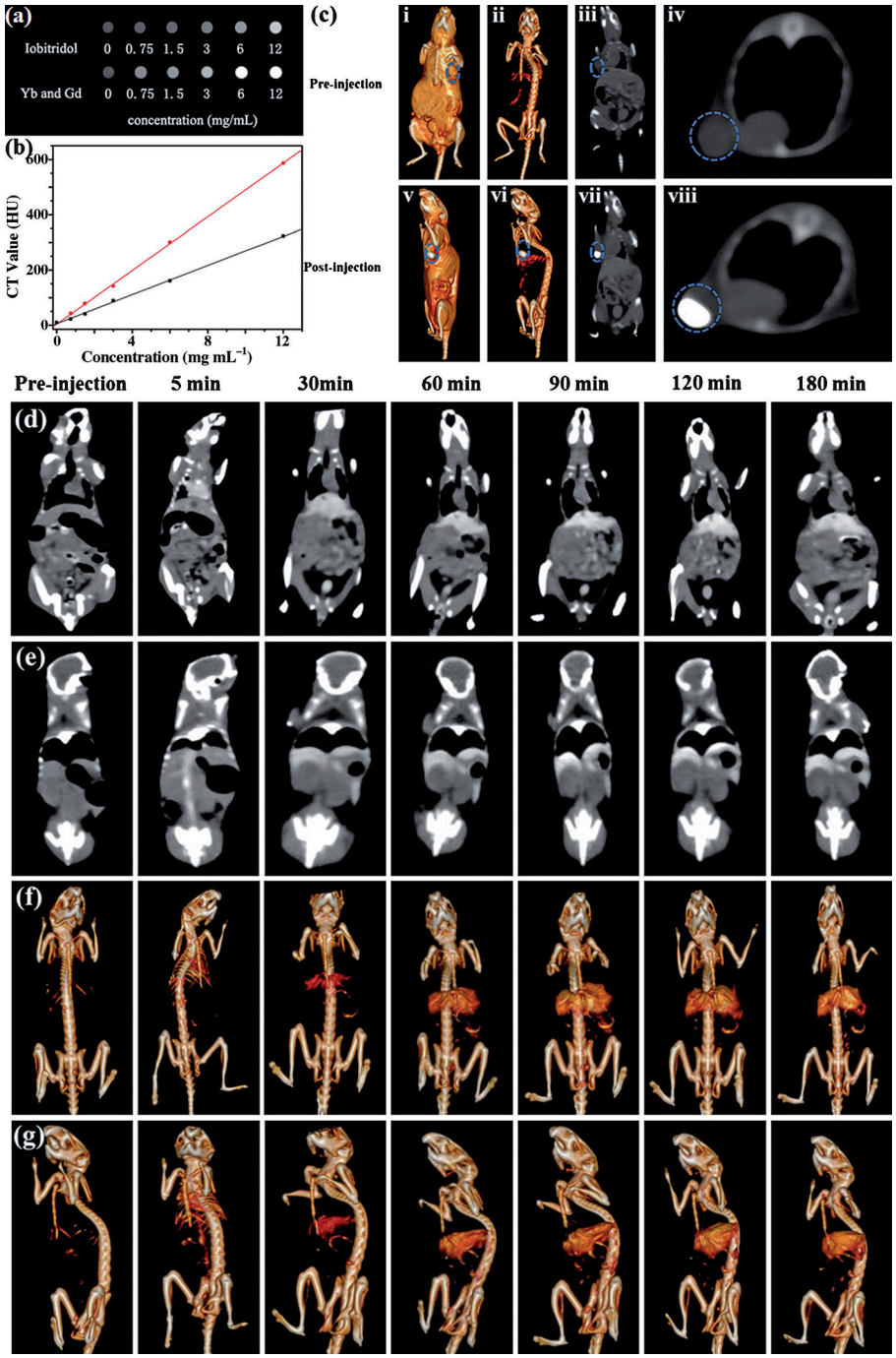

Figure 3. a) CT images of solutions of UCNPs@mSiO$_2$-ZnO and iobitridol with different concentrations. b) CT value (HU) of UCNPs@mSiO$_2$-ZnO (red circles) and iobitridol (black squares) as a function of the concentration. c) CT images of a tumor-bearing Balb/c mouse: pre-injection (i–iv) and after injection (v-viii) in situ. In vivo CT view images of a mouse after intravenous injection of UCNPs@mSiO$_2$-ZnO at timed intervals: d) heart and liver, e) spleen and kidney, f and g) the corresponding 3D renderings of in vivo CT images.

UCNPs@mSiO$_2$-ZnO, the tumor-bearing mouse shows significantly enhanced contrast of the tumors in the CT images (Figure 3c). The time-dependent biodistribution was tracked by CT signals after intravenous injection to evaluate the feasibility of UCNPs@mSiO$_2$-ZnO as an imaging probe in a mouse. Compared with the pre-injection CT imaging, it is seen in Figure 3d to g that the heart imaging was greatly enhanced after 5 minutes, and a clear imaging of the liver could be observed until 30 minutes, and was gradually increased from 30 to 120 minutes. More importantly, the enhancement of the liver imaging continued for over three hours. Such long-lasting hepatic enhancement probably reflected the uptake ability of UCNPs@mSiO$_2$-ZnO by macrophages and hepatocytes while used for probing hepatic tumors.[13] The results firmly demonstrate that the UCNPs@mSiO$_2$-ZnO effectively serve as a contrast agent for CT imaging both in vitro and in vivo.

Research on multifunctionalities of UCNPs@mSiO$_2$-ZnO was then extended to MRI for improving the resolution of soft tissues. Figure 4a displays the T_1-weighted relaxivity of UCNPs@mSiO$_2$-ZnO that the MRI contrast is enhanced by increasing the concentration of Gd^{3+} ions. The longitudinal relaxivity value (r_1) is calculated to be 4.78 mM^{-1}s^{-1} from the slope of the concentration-dependent relaxation $1/T_1$ (Figure 4b). The in vivo MRI experiment was conducted on a tumor-bearing mouse by using a 1.5 T human MRI scanner. After intratumoral injection of UCNPs@mSiO$_2$-ZnO into the tumor necrosis area, the enhanced MRI signal can be clearly observed in the injection area (Figure S10). The above tests identify that UCNPs@mSiO$_2$-ZnO can be successfully employed as a UCL/CT/MRI tri-modality imaging probe for tumor diagnosis.

UCNPs@mSiO$_2$-ZnO exhibited a strong green emission under irradiation with UV light in phosphate-buffered saline (PBS; pH 7.4), typically originated from surface-modified ZnO quantum dots, however, this emission was quickly quenched while pH 5.0, indicating the dissolution of ZnO quantum dots by acid (Figure S11). This judgement is in good consistence with the corresponding TEM and EDX characterization (Figures S12 and S13). Obviously the acid metabolized by tumors can easily open the "gate" guarded by ZnO to achieve pH-triggered on-demand drug release. In the following we choose an extensively used clinical chemotherapy drug doxorubicin

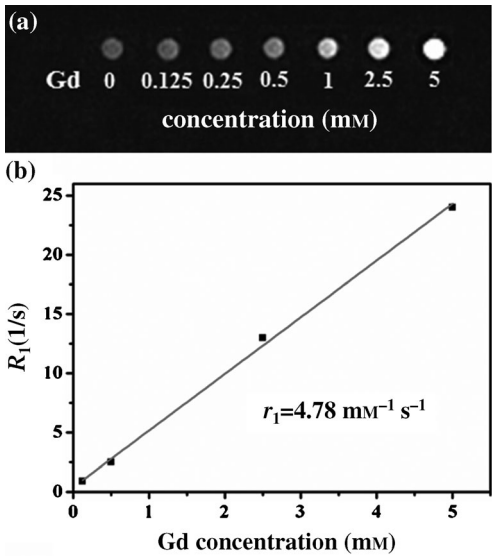

Figure 4. a) In vitro T_1-weighted MRI maps of UCNPs@mSiO$_2$-ZnO with varied Gd^{3+} concentrations. b) Plots of the relaxation rate R_1 versus different molar concentrations of Gd^{3+} ions.

(DOX) as a model and pre-loaded it in the mesopores of UCNPs@mSiO$_2$ at a content of 102 mg g^{-1} before the pore was guarded by ZnO quantum dots. The subsequent test of sustained release of the drug under different pH values in Figure 5a shows that an extremely slow drug release from UCNPs@mSiO$_2$@DOX-ZnO was detected at pH 7.4, suggesting ZnO worked well in preventing premature drug leakage. Oppositely, a remarkable drug release of DOX occurred at pH 5.0 in the very beginning until after seven hours a balanced concentration was reached. The control experiments without ZnO caps and with Au caps (stable at pH 5.0) were also performed (Figure S14), which further verify that ZnO quantum dots are excellent "gatekeepers" for controlling the drug release. The internalization of UCNPs@mSiO$_2$@DOX-ZnO into cancer cells and intracellular release of DOX were studied by inverted fluorescence microscopy (Figure S15). The fluorescent intensity enhancement of DOX in cancer cells increases with incubation time, indicating the sustained intracellular release of drugs from UCNPs@mSiO$_2$@DOX-ZnO. The anticancer efficacy of UCNPs@mSiO$_2$@DOX-ZnO was tested on the HeLa cancer cell line. Figure 5b shows the viabilities of HeLa cells against free DOX, UCNPs@mSiO$_2$, UCNPs@mSiO$_2$-ZnO, and UCNPs@mSiO$_2$@DOX-ZnO after incubation for 24 h. UCNPs@mSiO$_2$ shows limited cytotoxic effects on the cells even at the high concentration of 200 μg mL^{-1}, whereas UCNPs@mSiO$_2$-ZnO exhibited a statistically significant cytotoxic effect, indicating that ZnO exhibit cytotoxic effects after dissolution (Figure S16).[14] Moreover, UCNPs@mSiO$_2$@DOX-ZnO results in higher amounts of HeLa cell deaths than free DOX, which indicated that the loaded DOX not only retained its pharmaceutical activity but also exhibited a higher therapeutic effectiveness. The results prove the feasibility of UCNPs@mSiO$_2$@DOX-ZnO to effectively store and deliver DOX into cancer cells and further provide pH-triggered controlled release to induce cell death.

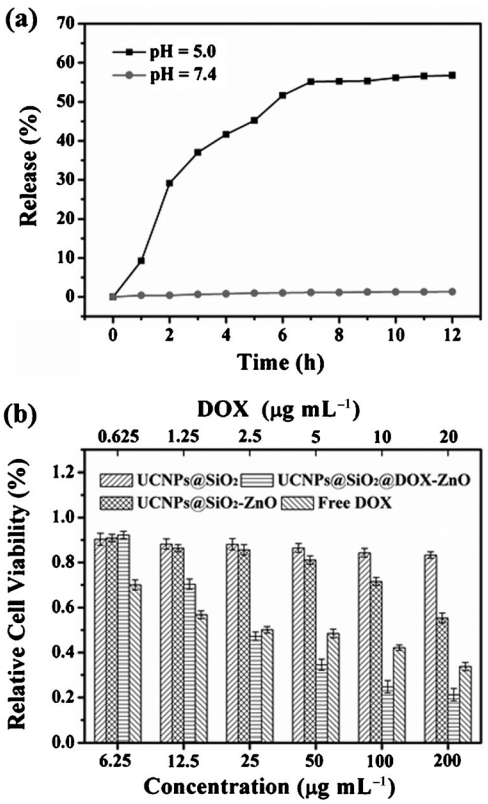

Figure 5. a) Release profiles of UCNPs@mSiO$_2$@DOX-ZnO at pH 7.4 and 5.0 at 37 °C. b) Cell viability of HeLa cells incubated with free DOX, UCNPs@mSiO$_2$, UCNPs@mSiO$_2$-ZnO, and UCNPs@mSiO$_2$@DOX-ZnO for 24 h, respectively.

In summary, a ZnO-gated UCNPs@mSiO$_2$ nanoplatform has been successfully constructed for multi-modality bioimaging and guided pH-triggered on-demand drug release. The combination studies of UCL imaging with CT and MRI reveal that UCNPs@mSiO$_2$-ZnO can well serve as contrast agents for tri-modal imaging in vitro and in vivo, providing comprehensive information for tumor diagnosis. More importantly, the "gatekeeper" ZnO can be efficiently dissolved in the acidic environment of cancer cells, and hence UCNPs@mSiO$_2$-ZnO cannot only effectively load anticancer drugs, but also achieve pH-triggered on-demand drug release, which effectually reduces adverse side effects of drugs. This nanoplatform has exhibited greater cytotoxicity than the corresponding free drugs, indicating their high therapeutic effectiveness for cancer. All these positive results make UCNPs@mSiO$_2$-ZnO nanocomposites a promising candidate for cancer theranostics, and it has inspired us much to develop novel effective imaging-guided on-demand chemotherapies in cancer treatment.

Received: September 26, 2014
Published online: November 3, 2014

Keywords: cancer · drug delivery · multi-modality imaging · upconverting nanoparticles · therapeutic agents

[1] a) J. Cheon, J. H. Lee, *Acc. Chem. Res.* **2008**, *41*, 1630; b) J. Kim, Y. Piao, T. Hyeon, *Chem. Soc. Rev.* **2009**, *38*, 372; c) S. M. Ametamey, M. Honer, P. A. Schubiger, *Chem. Rev.* **2008**, *108*, 1501; d) D. Patel, A. Kell, B. Simard, B. Xiang, H. Y. Lin, G. H. Tian, *Biomaterials* **2011**, *32*, 1167.

[2] a) S. T. Selvan, *Biointerphases* **2010**, *5*, FA110; b) Q. Ma, Y. Nakane, Y. Mori, M. Hasegawa, Y. Yoshioka, T. M. Watanabe, K. Gonda, N. Ohuchi, T. Jin, *Biomaterials* **2012**, *33*, 8486; c) A. J. Mieszawska, W. J. M. Mulder, Z. A. Fayad, D. P. Cormode, *Mol. Pharm.* **2013**, *10*, 831.

[3] a) Y. Dai, H. Xiao, J. Liu, Q. Yuan, P. Ma, D. Yang, C. Li, Z. Cheng, Z. Hou, P. Yang, J. Lin, *J. Am. Chem. Soc.* **2013**, *135*, 18920; b) X. Xie, N. Gao, R. Deng, Q. Sun, Q. Xu, X. Liu, *J. Am. Chem. Soc.* **2013**, *135*, 12608; c) Y. F. Wang, G. Y. Liu, L. D. Sun, J. W. Xiao, J. C. Zhou, C. H. Yan, *ACS Nano* **2013**, *7*, 7200; d) J. Wang, R. Deng1, M. A. MacDonald, B. Chen, J. Yuan, F. Wang, D. Chi, T. S. A. Hor, P. Zhang, G. Liu, Y. Han, X. Liu, *Nat. Mater.* **2014**, *13*, 157; e) Y. Sun, X. Zhu, J. Peng, F. Li, *ACS Nano* **2013**, *7*, 11290; f) Y. Yang, B. Velmurugan, X. Liu, B. Xing, *Small* **2013**, *9*, 2937.

[4] a) Y. Liu, K. Ai, J. Liu, Q. Yuan, Y. He, L. Lu, *Angew. Chem. Int. Ed.* **2012**, *51*, 1437; *Angew. Chem.* **2012**, *124*, 1466; b) H. Xing, S. Zhang, W. Bu, X. Zheng, L. Wang, Q. Xiao, D. Ni, J. Zhang, L. Zhou, W. Peng, K. Zhao, Y. Hua, J. Shi, *Adv. Mater.* **2014**, *26*, 3867.

[5] a) M. Haase, H. Schäfer, *Angew. Chem. Int. Ed.* **2011**, *50*, 5808; *Angew. Chem.* **2011**, *123*, 5928; b) Y. Yang, Q. Shao, R. Deng, C. Wang, X. Teng, K. Cheng, Z. Cheng, L. Huang, Z. Liu, X. Liu, B. Xing, *Angew. Chem. Int. Ed.* **2012**, *51*, 3125; *Angew. Chem.* **2012**, *124*, 3179; c) R. Deng, X. Xie, M. Vendrell, Y.-T. Chang, X. Liu, *J. Am. Chem. Soc.* **2011**, *133*, 20168; d) W. Wu, L. Yao, T. Yang, R. Yin, F. Li, Y. Yu, *J. Am. Chem. Soc.* **2011**, *133*, 15810; e) F. Vetrone, R. Naccache, V. Mahalingam, C. G. Morgan, J. A. Capobianco, *Adv. Funct. Mater.* **2009**, *19*, 2924; f) K. G. Jayakumar, N. M. Idris, Y. Zhang, *Proc. Natl. Acad. Sci. USA* **2012**, *109*, 8483; g) Q. Zhan, J. Qian, H. Liang, G. Somesfalean, D. Wang, S. He, Z. Zhang, S. Andersson-Engels, *ACS Nano* **2011**, *5*, 3744; h) Y. I. Park, H. M. Kim, J. H. Kim, K. C. Moon, B. Yoo, K. T. Lee, N. Lee, Y. Choi, W. Park, D. Ling, K. Na, W. K. Moon, S. H. Choi, H. S. Park, S.-Y. Yoon, Y. D. Suh, S. H. Lee, T. Hyeon, *Adv. Mater.* **2012**, *24*, 5755.

[6] a) K. Liu, X. Liu, Q. Zeng, Y. Zhang, L. Tu, T. Liu, X. Kong, Y. Wang, F. Cao, S. A. G. Lambrechts, M. C. G. Aalders, H. Zhang, *ACS Nano* **2012**, *6*, 4054; b) Y. Wang, H. Wang, D. Liu, S. Song, X. Wang, H. Zhang, *Biomaterials* **2013**, *34*, 7715; c) Q. Xiao, X. Zheng, W. Bu, W. Ge, S. Zhang, F. Chen, H. Xing, Q. Ren, W. Fan, K. Zhao, Y. Hua, J. Shi, *J. Am. Chem. Soc.* **2013**, *135*, 13041; d) Q. Chen, C. Wang, L. Cheng, W. He, Z. Cheng, Z. Liu, *Biomaterials* **2014**, *35*, 2915.

[7] a) Z. Hou, C. Li, P. Ma, Z. Cheng, X. Li, X. Zhang, Y. Dai, D. Yang, H. Lian, J. Lin, *Adv. Funct. Mater.* **2012**, *22*, 2713; b) W. Fan, B. Shen, W. Bu, F. Chen, K. Zhao, S. Zhang, L. Zhou, W. Peng, Q. Xiao, H. Xing, J. Liu, D. Ni, Q. He, J. Shi, *J. Am. Chem. Soc.* **2013**, *135*, 6494; c) S. Gai, P. Yang, C. Li, W. Wang, Y. Dai, N. Niu, J. Lin, *Adv. Funct. Mater.* **2010**, *20*, 1166.

[8] a) G. Tian, W. Yin, J. Jin, X. Zhang, G. Xing, S. Li, Z. Gu, Y. Zhao, *J. Mater. Chem. B* **2014**, *2*, 1379; b) C. Wang, L. Cheng, Z. Liu, *Biomaterials* **2011**, *32*, 1110.

[9] a) J. Liu, W. Bu, L. Pan, J. Shi, *Angew. Chem. Int. Ed.* **2013**, *52*, 4375; *Angew. Chem.* **2013**, *125*, 4471; b) L. Zhao, J. Peng, Q. Huang, C. Li, M. Chen, Y. Sun, Q. Lin, L. Zhu, F. Li, *Adv. Funct. Mater.* **2014**, *24*, 363.

[10] a) Y. Dai, P. Ma, Z. Cheng, X. Kang, X. Zhang, Z. Hou, C. Li, D. Yang, X. Zhai, J. Lin, *ACS Nano* **2012**, *6*, 3327; b) X. Zhang, P. Yang, Y. Dai, P. Ma, X. Li, Z. Cheng, Z. Hou, X. Kang, C. Li, J. Lin, *Adv. Funct. Mater.* **2013**, *23*, 4067.

[11] a) D. Yang, Y. Dai, P. Ma, X. Kang, Z. Cheng, C. Li, J. Lin, *Chem. Eur. J.* **2013**, *19*, 2685; b) C. Li, D. Yang, P. Ma, Y. Chen, Y. Wu, Z. Hou, Y. Dai, J. Zhao, C. Sui, J. Lin, *Small* **2013**, *9*, 4150.

[12] a) F. Muhammad, M. Guo, W. Qi, F. Sun, A. Wang, Y. Guo, G. Zhu, *J. Am. Chem. Soc.* **2011**, *133*, 8778; b) Z. Zhang, Y. Xu, Y. Ma, L. Qiu, Y. Wang, J. Kong, H. Xiong, *Angew. Chem. Int. Ed.* **2013**, *52*, 4127; *Angew. Chem.* **2013**, *125*, 4221; c) H. Xiong, *Adv. Mater.* **2013**, *25*, 5329; d) H. Yang, H. Xiong, S. Yu, *Process. Chem.* **2012**, *24*, 2234; e) Z. Pan, J. Liang, Z. Zheng, H. Wang, H. Xiong, *Contrast Media Mol. Imaging* **2011**, *6*, 378; f) H. Xiong, Y. Xu, O. Ren, Y. Xia, *J. Am. Chem. Soc.* **2008**, *130*, 7522.

[13] a) M. C. Woodle, C. M. Engbers, S. Zalipsky, *Bioconjugate Chem.* **1994**, *5*, 493; b) D. Kim, S. Park, J. H. Lee, Y. Y. Jeong, S. Jon, *J. Am. Chem. Soc.* **2007**, *129*, 7661.

[14] a) K. H. Müller, J. Kulkarni, M. Motskin, A. Goode, P. Winship, J. N. Skepper, M. P. Ryan, A. E. Porter, *ACS Nano* **2010**, *4*, 6767; b) T. Xia, M. Kovochich, M. Liong, L. Mädler, B. Gilbert, H. B. Shi, J. I. Yeh, J. I. Zink, A. E. Nel, *ACS Nano* **2008**, *2*, 2121; c) A. E. Nel, L. Mädler, D. Velegol, T. Xia, E. M. V. Hoek, P. Somasundaran, F. Klaessig, V. Castranova, M. Thompson, *Nat. Mater.* **2009**, *8*, 543.

